Support Information for Theoretical Design of Two-dimensional $AMInP_2X_3Y_3$ (AM = Li, Na, K; X/Y = S, Se, Te) monolayers for highly efficient excitonic solar cells

Linlin Liu,[a] Yu Xie,[*a,b], John S.Tse,[*a,c] and Yanming Ma,[a,d]

1 Computational method

The solar-to-hydrogen (STH) efficiency[1,2] is determined as

$$\eta_{STH} = \eta_{abs} \times \eta_{cu} \tag{1}$$

where η_{abs} is the light absorption efficiency, η_{cu} is the carrier utilization. And the efficiency of optical absorption is calculated by the following expression:

$$\eta_{abs} = \frac{\int_{E_g}^{\infty} P(h\omega)d(h\omega)}{\int_{0}^{\infty} P(h\omega)d(h\omega} \tag{2}$$

where $P(h\omega)$ is the AM1.5G solar energy flux[3] at the photon energy $h\omega$ and E_{g} is the band gap of semiconductor materials. The efficiency of carrier utilization is defined as

$$\eta_{cu} = \frac{\Delta G \int_{E}^{\infty} \frac{P(h\omega)}{h\omega} d(h\omega)}{\int_{E_g}^{\infty} P(h\omega)d(h\omega} \tag{3}$$

where ΔG is the potential difference between the redox potentials of and H_2O/O_2 and H^+/H_2 of 1.23 eV for water splitting. E is the minimum energy of photons that can be used for water splitting. Considering energy barriers of both HER and OER[4,5], E can be defined as

$$E = \begin{cases} E_g, (\chi(H_2) \geq 0.2, \chi(O_2) \geq 0.6) \\ E_g + 0.2 - \chi(H_2), (\chi(H_2) < 0.2, \chi(O_2) \geq 0.6) \\ E_g + 0.6 - \chi(O_2), (\chi(H_2) \geq 0.2, \chi(O_2) < 0.6) \\ E_g + 0.8 - \chi(O_2) - \chi(H_2), (\chi(H_2) < 0.2, \chi(O_2) < 0.6) \end{cases} \tag{4}$$

$\chi(H_2)$ is the energy difference between redox potentials H^+/H_2 and CBM. $\chi(O_2)$ is the energy difference between redox potentials H_2O/O_2 and VBM.

The thermodynamics of water splitting on 2D $AMInP_2X_3Y_3$ monolayers are estimated by examining the HER and OER processes. We marked $*$, H^*, OH^*, O^*, OOH^* as the bare surface, and HER, OER intermediates adsorbed on the 2D $AMInP_2X_3Y_3$ monolayers. l and g refer to liquid and gas phases, respectively.

The overall hydrogen evolution reaction under standard conditions can be described as follows:

$$* + H^+ + e^- \rightarrow H* \tag{5}$$

$$H* + H^+ + e^- \rightarrow H_2 + * \tag{6}$$

While for OER, the four-electron process is interpreted as following four elementary steps:

$$* + H_2O \rightarrow OH* + H^+ + e^- \tag{7}$$

[a]International Center for Computational Method & Software and State Key Laboratory of Superhard Materials, College of Physics, Jilin University, Changchun, 130012, China
[b]Key Laboratory of Physics and Technology for Advanced Batteries (Ministry of Education), Jilin University, Changchun, 130012, China. E-mail: xieyu@jlu.edu.cn
[c]Department of Physics and Engineering Physics, University of Saskatchewan, Saskatoon, SK S7N 5E2, Canada. E-mail: john.tse@usask.ca
[d]International Center of Future Science, Jilin University, 130012 Changchun, China. E-mail: mym@jlu.edu.cn

Table S1 Values used for the entropy and zero-point energy corrections in determining the free energy of reactants, products, and intermediate species adsorbed on catalysts[7].

Species	T × S (eV)	ZPE (eV)
H*	0	0.17
O*	0.06	0.07
OH*	0.08	0.33
OOH*	0.21	0.43
H_2(g)	0.41	0.27
H_2O(g)	0.58	0.57

$$OH* \rightarrow O^* + H^+ + e^- \tag{8}$$

$$O* + H_2O \rightarrow OOH* + H^+ + e^- \tag{9}$$

$$OOH* \rightarrow * + O_2 + H^+ + e^- \tag{10}$$

For each reaction of both oxidation and hydrogen production, the free energy is different under the effect of pH and an extra potential bias can be written as:

$$\Delta G = \Delta E + \Delta ZPE - T\Delta S + \Delta G_{pH} + \Delta G_U \tag{11}$$

The ΔE, ΔZPE, and ΔS are different energy, zero-point energy, and entropy of the reaction, respectively. The ΔE is obtained from DFT calculation, while the ΔZPE, and ΔS are calculated from the values of Table S1. The entropies of free molecules can be found in the NIST database[6]. As the DFT method cannot accurately describe the high-spin ground state of the O_2 molecule, the Gibbs free energy of O_2 [G_{O_2}] is obtained by G_{O_2} = $2G_{H_2O}$ - $2G_{H_2}$ + 4.92. T represents indoor temperature in this work. ΔG_{pH} ($\Delta G_{pH} = k_B T \times \ln 10 \times pH$) represents the free energy contributed in different pH concentrations. ΔG_U (ΔG_U = -eU) denotes extra potential bias provided by an electron in the electrode, where U is the electrode potential relative to the standard hydrogen electrode (SHE). ΔG_U refers to the Gibbs free energy change imposed by light-induced driven potential (U) and equals -eU. The light-induced driven potential for HER can be obtained by U_e = [E_{CBM} - (-4.44 + 0.059 × pH)]/e, and the driven potential for OER is determined by U_h = [-E_{VBM} + (-4.44 + 0.059 × pH)]/e. E_{VBM} and E_{CBM} represent the energy level of the valance band maximum (VBM) and conduction band minimum (CBM) of the photocatalysts, respectively. Both the VBM and CBM were regulated by the vacuum level.

$$\Delta G_1 = G_{H*} - \frac{1}{2}G_{H_2} - G* + \Delta G_U + \Delta G_{pH} \tag{12}$$

$$\Delta G_2 = G_* + \frac{1}{2}G_{H_2} - G_{H*} + \Delta G_U + \Delta G_{pH} \tag{13}$$

$$\Delta G_3 = G_{OH*} + \frac{1}{2}G_{H_2} - G_* - G_{H_2O} + \Delta G_U - \Delta G_{pH} \tag{14}$$

$$\Delta G_4 = G_{O*} + \frac{1}{2}G_{H_2} - G_{OH*} + \Delta G_U - \Delta G_{pH} \tag{15}$$

$$\Delta G_5 = G_{OOH*} + \frac{1}{2}G_{H_2} - G_{O*} - G_{H_2O} + \Delta G_U - \Delta G_{pH} \tag{16}$$

$$\Delta G_6 = G_* + \frac{1}{2}G_{H_2} + G_{O_2} - G_{OOH*} + \Delta G_U - \Delta G_{pH} \tag{17}$$

We calculated the orientation-dependent Poisson's ratio $\upsilon(\theta)$ and Young's modulus $Y(\theta)$ for the lowest energy phase in 2D $AMInP_2X_3Y_3$ monolayers by using the following equations

.

$$Y(\theta) = \frac{C_{11}C_{22} - C_{12}^2}{C_{11}sin^4(\theta) + Asin^2(\theta)cos^2(\theta) + C_{22}cos^4(\theta)} \tag{18}$$

$$\upsilon(\theta) = \frac{C_{12}sin^4(\theta) - Bsin^2(\theta)cos^2(\theta) + C_{12}cos^4(\theta)}{C_{11}sin^4(\theta) + Asin^2(\theta)cos^2(\theta) + C_{22}cos^4(\theta)} \tag{19}$$

where A=($C_{11}C_{22}$-C_{12}^2)/C_{66} -2C_{12} and B = C_{11}+C_{22}-($C_{11}C_{22}$-C_{12}^2)/C_{66}.

2 Structure and Stability

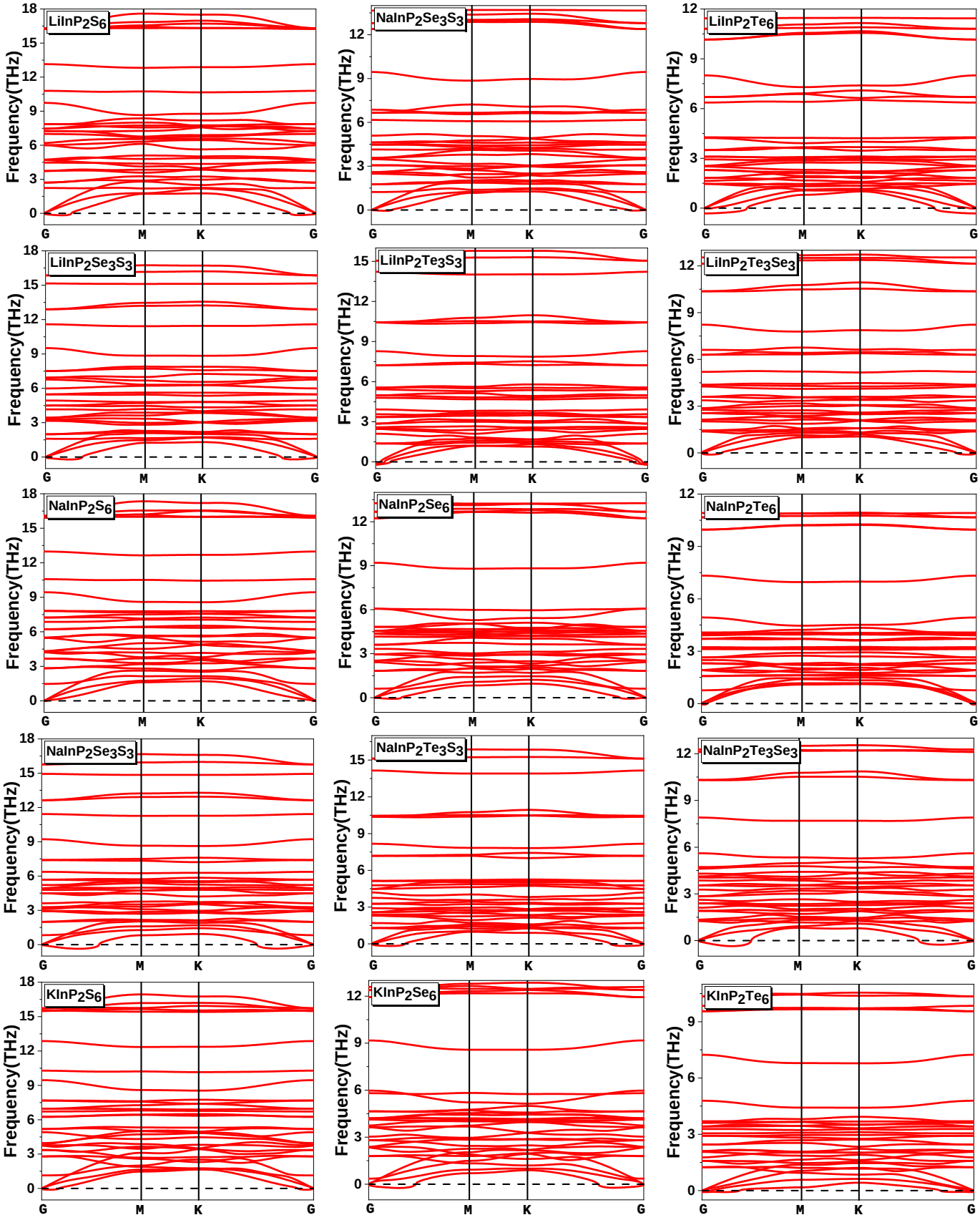

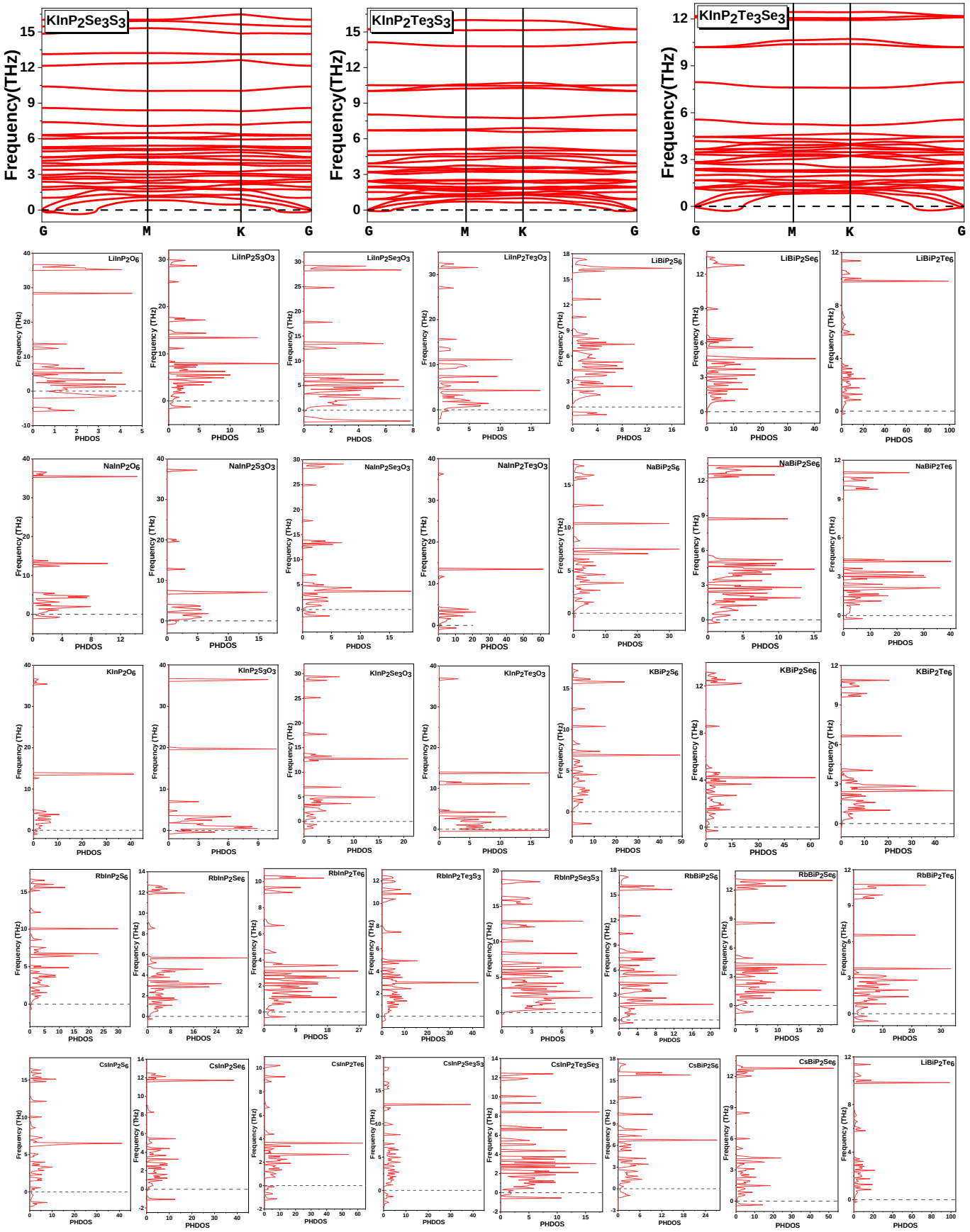

Fig. S1 The calculated phonon dispersions spectras and PhDOS of 2D $AMInP_2X_6$ and $AMInP_2X_3Y_3$ monolayers.

Table S2 Stable 2D $AMInP_2X_6$ and $AMInP_2X_3Y_3$ monolayers: lattice constant a(Å), material thickness h(Å); formation energy E_{form} and cohesive energy E_{coh} (eV), in-plane stiffness (or in-plane Young's modulus): C (N/m), Poisson's ratio ν.

	a	h	E_{form}	E_{coh}	C_{11}	C_{12}	C_{66}	C	ν
$LiInP_2S_6$	6.16	3.33	-0.53	3.55	53.05	13.74	19.66	49.50	0.26
$LiInP_2Se_6$	6.52	3.51	-0.43	3.16	43.91	11.67	16.12	40.81	0.27
$LiInP_2Se_3S_3$	6.34	3.41	-0.47	3.34	49.94	13.37	18.29	46.37	0.27
$LiInP_2Te_3S_3$	6.64	3.50	-0.31	3.10	47.03	13.63	16.70	43.08	0.29
$LiInP_2Te_3Se_3$	6.78	3.59	-0.28	2.92	44.27	12.30	15.99	40.86	0.28
$NaInP_2S_6$	6.34	3.43	-0.51	3.48	47.56	14.08	16.74	43.39	0.30
$NaInP_2Se_6$	6.68	3.62	-0.41	3.09	39.30	12.64	13.33	35.24	0.32
$NaInP_2Te_6$	7.24	3.88	-0.14	2.64	29.30	11.27	9.02	24.97	0.38
$NaInP_2Se_3S_3$	6.50	3.50	-0.45	3.28	44.43	13.95	15.24	40.05	0.31
$NaInP_2Te_3S_3$	6.76	3.54	-0.32	3.05	45.83	17.45	14.19	39.18	0.38
$NaInP_2Te_3Se_3$	6.92	3.65	-0.27	2.86	41.35	15.08	13.17	35.85	0.36
$KInP_2S_6$	6.56	3.52	-0.51	3.44	45.00	17.17	13.92	38.44	0.38
$KInP_2Se_6$	6.90	3.72	-0.42	3.08	36.83	15.30	10.76	30.47	0.42
$KInP_2Te_6$	7.44	3.99	-0.18	2.66	26.52	14.05	6.23	19.07	0.53
$KInP_2Se_3S_3$	6.65	3.53	-0.47	3.27	41.11	15.37	12.87	35.36	0.37
$KInP_2Te_3S_3$	6.85	3.57	-0.35	3.06	31.78	29.57	1.10	4.26	0.93
$KInP_2Te_3Se_3$	7.05	3.67	-0.29	2.86	37.60	16.74	10.45	30.15	0.45

3 The mechanical stability of the stable 2D $AMInP_2X_3Y_3$ monolayers phases

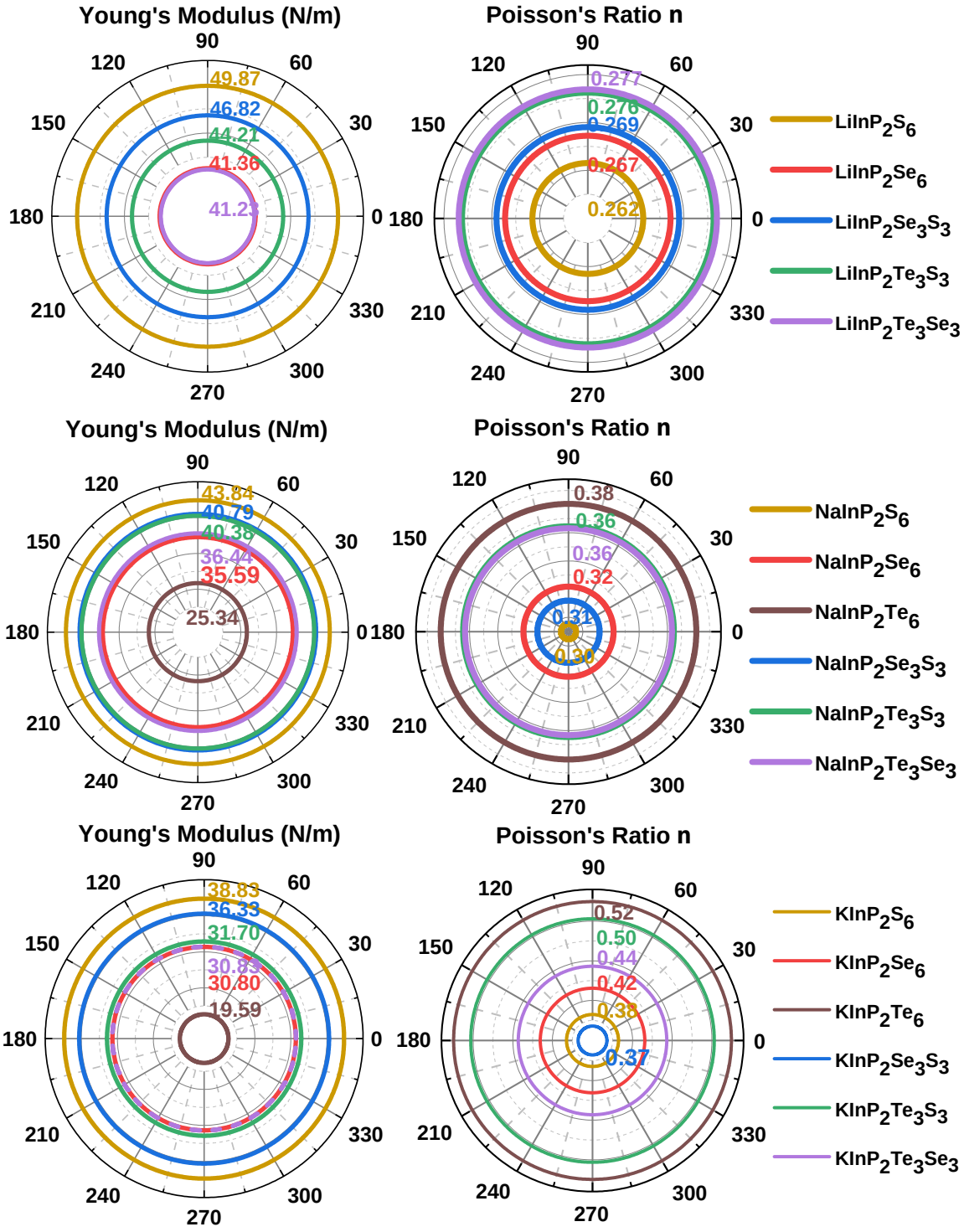

Fig. S2 Calculated orientation-dependent Young's modulus ($Y(\theta)$) (left panels) and Poisson's ratio ($\upsilon(\theta)$) (right panels).

4 The electronic band structure of the stable 2D $AMInP_2X_3Y_3$ monolayers phases

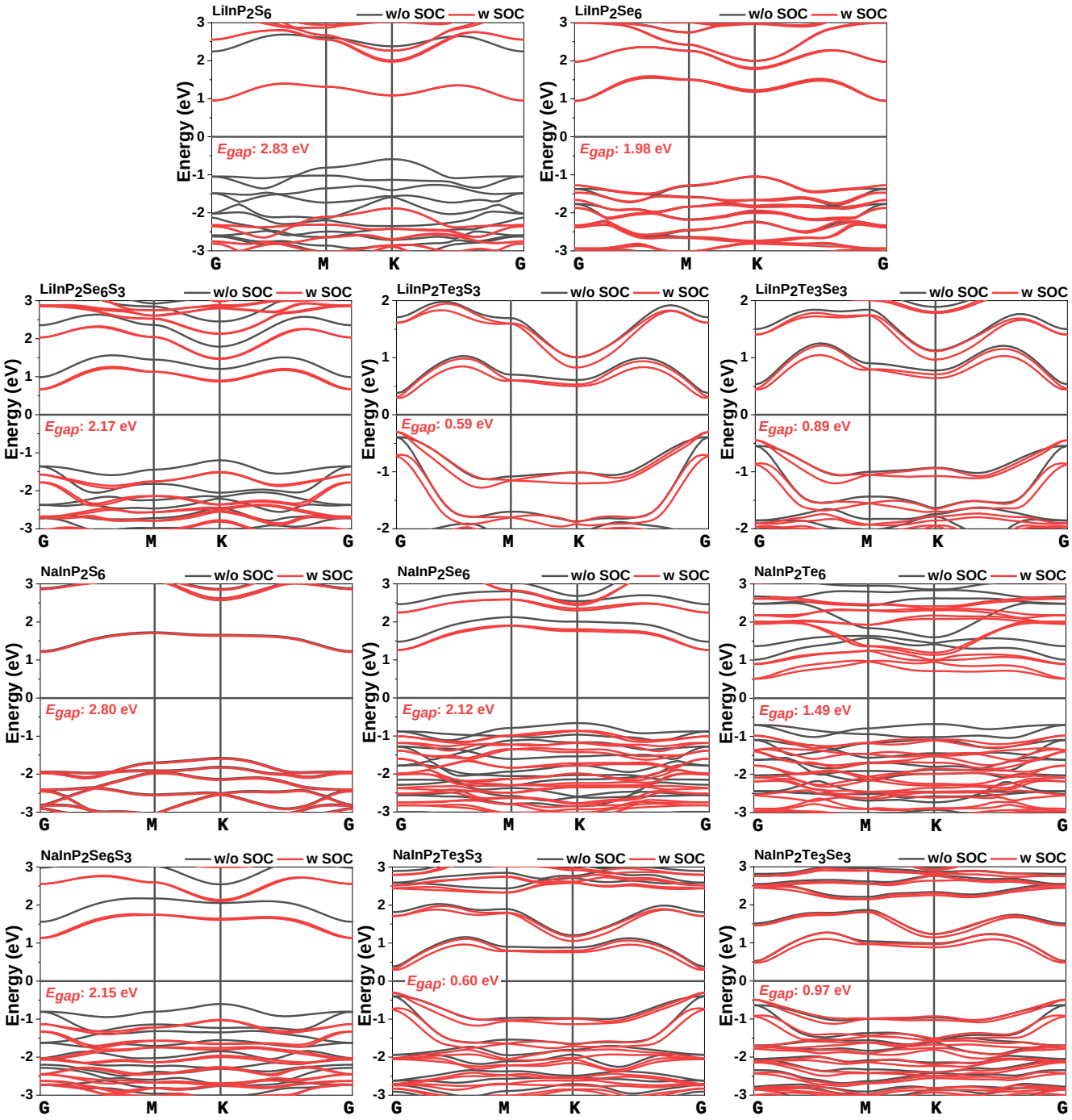

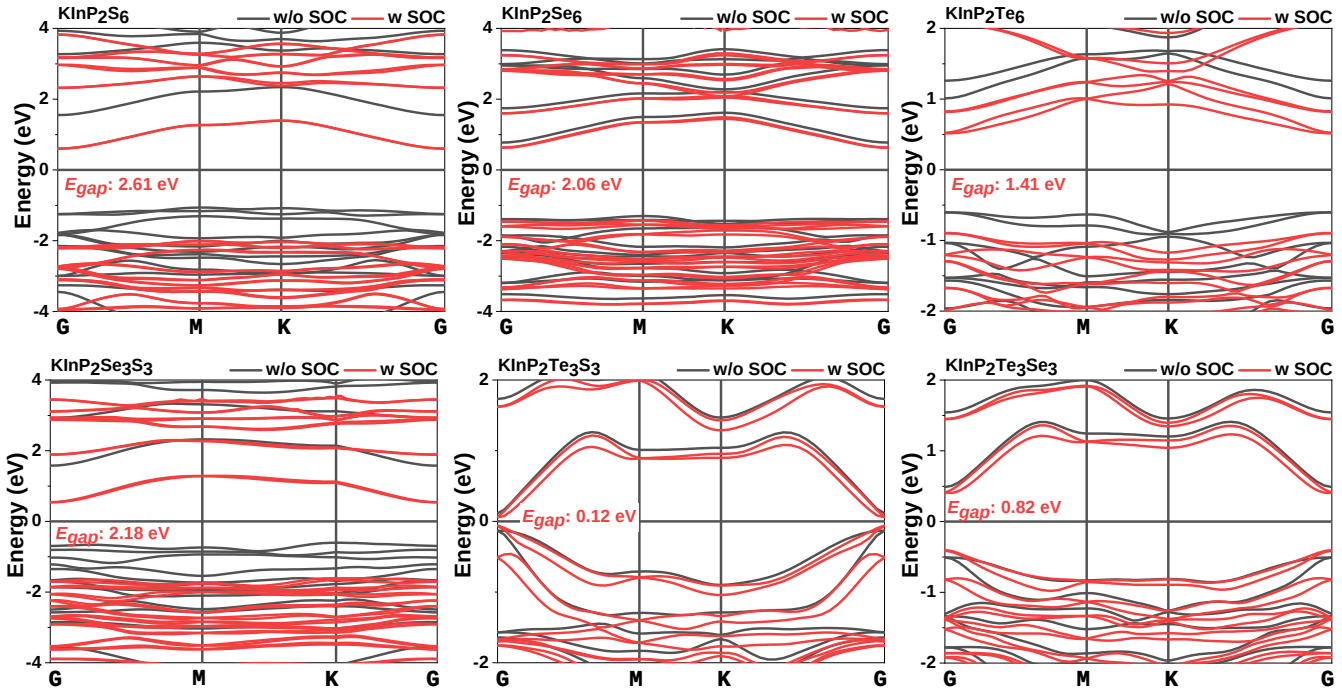

Fig. S3 Electronic band structure of $AMInP_2X_6$ and $AMInP_2X_3Y_3$ monolayers without (black line) and with spin-orbit coupling (SOC) (red line) at the HSE06 hybrid functional level of theory.

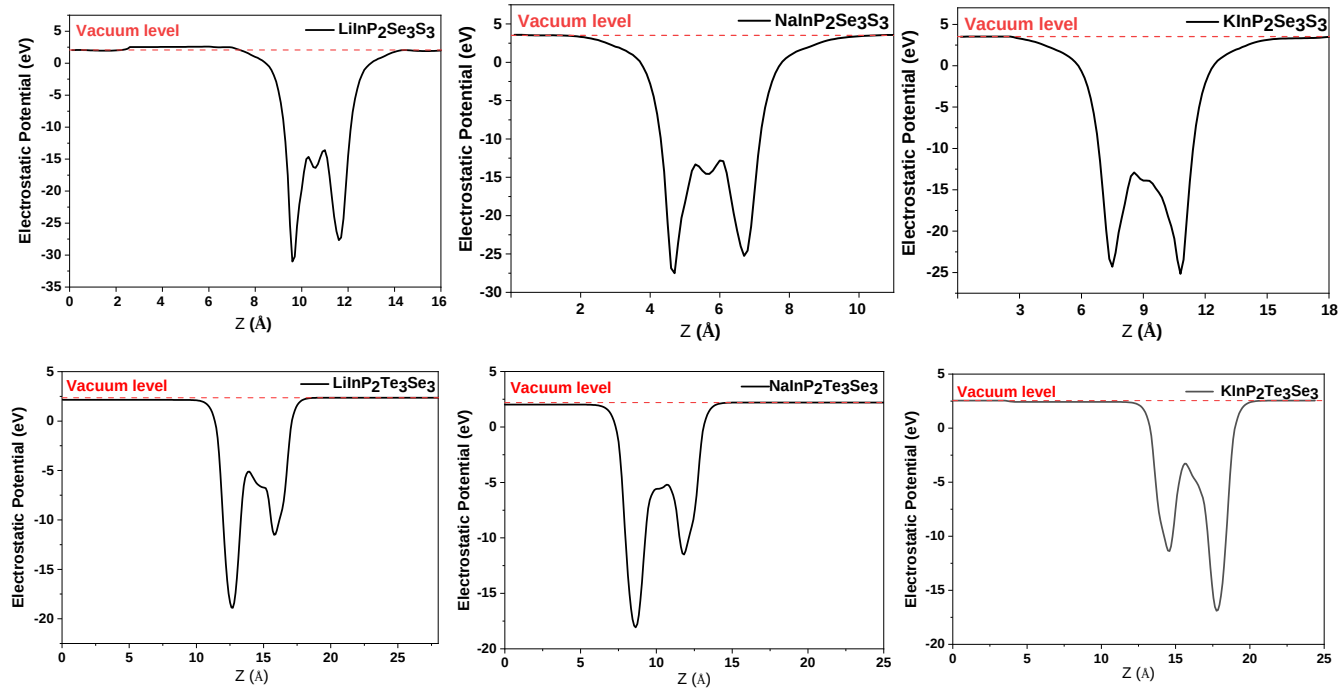

Fig. S4 Planar average electrostatic potential energy of $AMInP_2Se_3S_3$ and $AMInP_2Te_3Se_3$ monolayers.

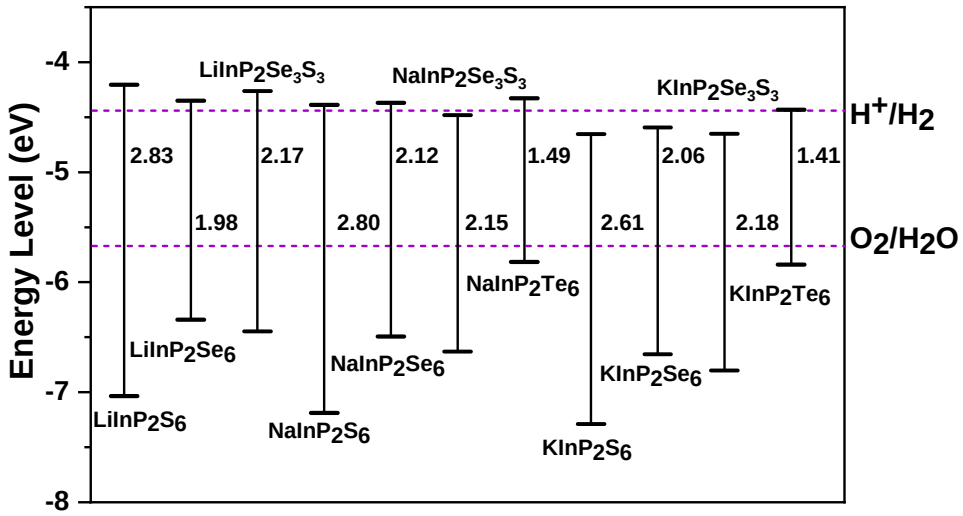

Fig. S5 Band edge positions with water redox potential for water splitting at pH = 0 for $AMInP_2X_6$, $LiInP_2Se_3S_3$, $NaInP_2Se_3S_3$ monolayers along the z-direction based on the HSE06 level of theory.

5 Convergence test

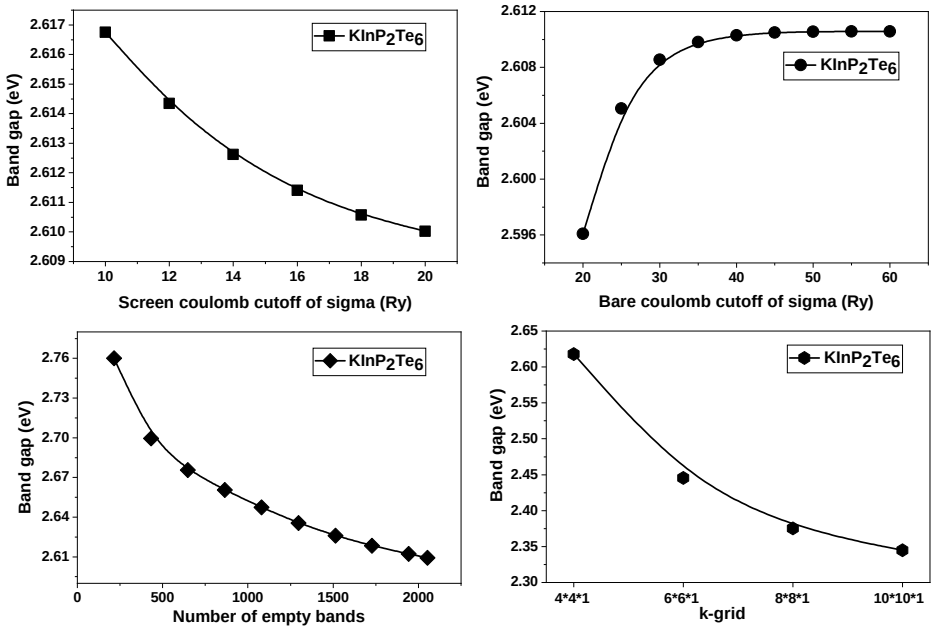

Fig. S6 Convergence of band gap to the kinetic energy cutoff, the bare coulomb cutoff of sigma, the screened cutoff of sigma, k-point sampling for $KInP_2Te_6$ monolayer.

6 Van der Waals heterostructures

In order to ensure thermodynamical stability, the binding energy is an essential parameter to be determined. The binding energy of the vdW heterostructures (vdWH) is evaluated as $E_b = \frac{E_{hetero} - E_{top} - E_{down}}{A}$, where E_{hetero} is the total energy of the vdWH, E_{top} and E_{down} represent the total energy of the pristine top and bottom monolayers (for the supercell having the same lattice parameters as that of the vdWH) and A is the area of the vdWH.

Table S3 The conduction band offsets (CBO) (ΔE_c) with SOC, lattices mismatch, interlayer distance (d), and binding energy of heterostructures. Power conversion efficiency (PCE) of proposed 2D heterostructure solar cells without/with SOC. A blank position means no heterostructured solar cell can be constructed.

Materials	CBO (eV)	Lattice mismatch (%)	d (Å)	E_b (meV/Å^2)	PCE (%) without SOC	PCE (%) with SOC
$NaInP_2Te_6/KInP_2Te_6$	0.10	0.80	2.50	-1.38	17.42	21.33
$NaInP_2Te_6/NaInP_2Te_3Se_3$	0.39	0.50	2.75	-1.60		16.43
$NaInP_2Te_6/CrS_2$	0.23	0.70	3.50	-1.97	11.08	13.30
$NaInP_2Te_6/MoGe_2N_4$	0.37	0.30	3.25	-1.18		16.04
$NaInP_2Te_6/PtS_2$	0.10	0.10	2.75	-1.67	17.42	21.53
$NaInP_2Te_6/InSe$	0.06	0.20	3.50	-68.61	17.57	22.12
$KInP_2Te_6/NaInP_2Te_3Se_3$	0.29	0.40	3.50	-0.72		17.80
$KInP_2Te_6/MoGe_2N_4$	0.27	0.40	2.75	-1.09		18.23
$LiInP_2Te_3Se_3/NaInP_2Te_3Se_3$	0.15	0.40	3.00	-0.59	18.84	16.80
$LiInP_2Te_3Se_3/KInP_2Te_3Se_3$	0.30	0.10	2.75	-0.42	14.33	10.45
$LiInP_2Te_3Se_3/CrS_2$	0.27	0.04	2.75	-0.29	13.73	11.16
$LiInP_2Te_3Se_3/PdSe_2$	0.23	0.60	3.25	-1.08	14.93	12.57
$LiInP_2Te_3Se_3/HfSe_2$	0.32	0.07	2.50	-2.39	20.05	9.40
$LiInP_2Te_3Se_3/MoGe_2N_4$	0.13	0.30	3.50	-0.46		16.10
$NaInP_2Te_3Se_3/CrS_2$	0.12	0.40	3.25	-0.69	19.46	20.87
$NaInP_2Te_3Se_3/PdSe_2$	0.12	0.20	2.50	-0.84	20.60	18.55
$NaInP_2Te_3Se_3/HfSe_2$	0.12	0.03	2.50	-0.63		15.51
$NaInP_2Te_3Se_3/MoGe_2N_4$	0.12	0.07	2.50	-0.55		21.93
$NaInP_2Te_3Se_3/BiIO$	0.12	0.30	2.50	-0.51	13.50	11.45
$NaInP_2Te_3Se_3/KInP_2Te_3Se_3$	0.12	0.08	2.50	-0.67	20.02	16.18
$KInP_2Te_3Se_3/HfSe_2$	0.02	0.90	3.50	-0.65		18.00
$KInP_2Te_3Se_3/BiIO$	0.15	0.03	2.75	-0.46		13.28
$KInP_2Te_3Se_3/HfS_2$	0.16	0.20	3.00	-0.65		12.92
$KInP_2Te_3Se_3/CrS_2$					22.14	

7 Photocatalytic Water Splitting

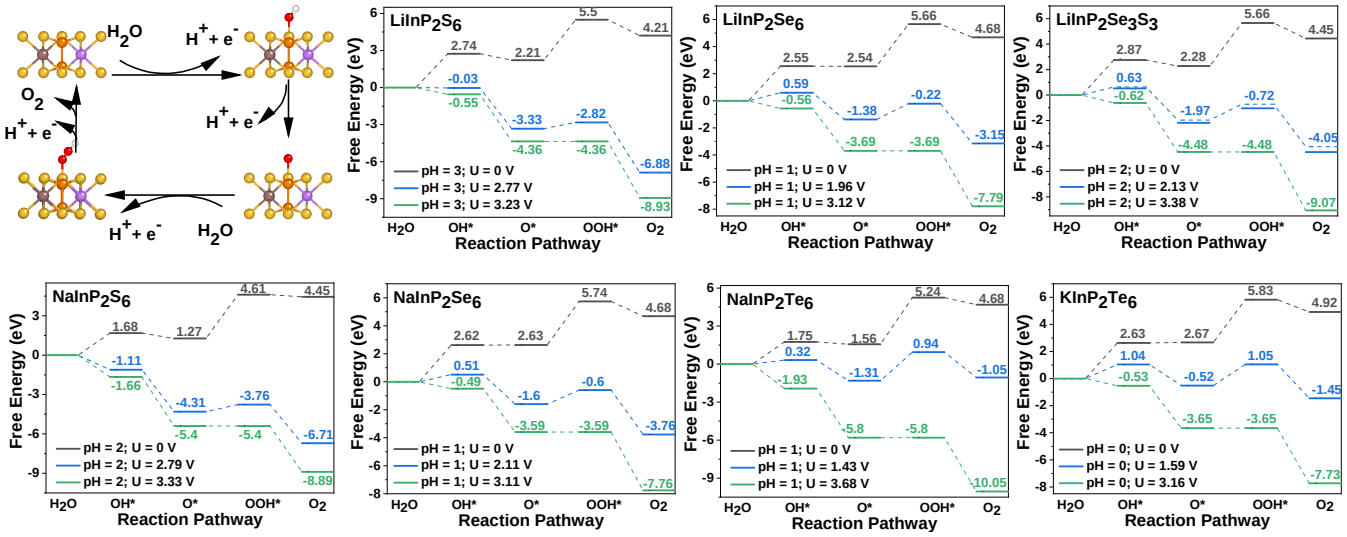

Fig. S7 Proposed photocatalytic pathways of water oxidation half-reactions with the most energetically favorable absorbed intermediates (OH^*, O^*, and OOH^*) in the $LiInP_2S_6$ monolayer. The red and white balls represent O and H atoms, respectively. Gibbs free energy (ΔG) vs. reaction coordinate for water oxidation half-reactions in $AMInP_2X_6$ and $LiInP_2Se_3Se_3$ monolayers applied at pH = 0 under different potentials. The value of ΔG in each elementary step is also shown. The blue lines denote the free energy of OERs under the external voltage supplied by photoexcited carriers.

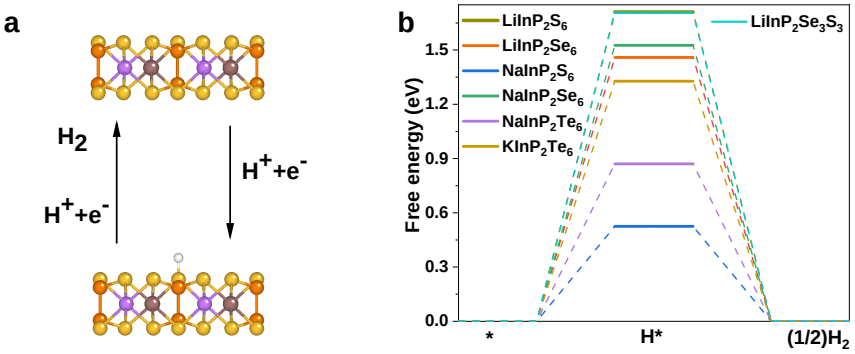

Fig. S8 Proposed photocatalytic pathways along with the atomic configuration of hydrogen reduction (a). The green ball represents the H atom. Gibbs free energy (ΔG) vs. reaction coordinate for hydrogen reduction half-reactions in $AMInP_2X_6$ and $LiInP_2Se_3Se_3$ monolayers applied at pH = 0 at potential U = 0.

Notes and references

1 Z. B. Chen, T. F. Jaramillo, T. G. Deutsch, A. Kleiman-Shwarsctein, A. J. Forman, N. Gaillard, R. Garland, K. Takanabe, C. Heske, M. Sunkara, E. W. McFarland, K. Domen, E. L. Miller, J. A. Turner and H. N. Dinh, *J. Mater. Res.*, 2010, **25**, 3–16.

2 Z. B. Chen, T. F. Jaramillo, T. G. Deutsch, A. Kleiman-Shwarsctein, A. J. Forman, N. Gaillard, R. Garland, K. Takanabe, C. Heske, M. Sunkara, E. W. McFarland, K. Domen, E. L. Miller, J. A. Turner and H. N. Dinh, *J. Mater. Res.*, 2010, **25**, 3–16.

3 C. A. Gueymard, *Solar Energy*, 2004, **76**, 423–453.

4 C. C. L. McCrory, S. H. Jung, J. C. Peters and T. F. Jaramillo, *J. Am. Chem. Soc.*, 2013, **135**, 16977–16987.

5 Y. Zheng, Y. Jiao, M. Jaroniec and S. Z. Qiao, *Angew. Chem., Int. Ed.*, 2015, **54**, 52–65.

6 R. D. Johnson, *Abstracts of Papers of the American Chemical Society*, 2005, **230**, U1015–U1015.

7 H. Xu, D. Cheng, D. Cao and X. C. Zeng, *Nat. Catal.*, 2018, **1**, 339–348.